Regulation of peroxisome and lipid droplet hitchhiking by PxdA and the DipA phosphatase

John Salogiannis[1,2*], Jenna R. Christensen[1*], Adriana Aguilar-Maldonado[1], Nandini Shukla[3,4,#], and Samara L. Reck-Peterson[1,2,5]

[1] Department of Cellular and Molecular Medicine, University of California San Diego, La Jolla, CA
[2] Howard Hughes Medical Institute, Chevy Chase, MD
[3] The Ohio State Biochemistry Program, The Ohio State University, Columbus, OH
[4] Department of Molecular Genetics, The Ohio State University, Columbus, OH
[5] Section of Cell and Developmental Biology, Division of Biological Sciences, University of California San Diego, La Jolla, CA

[*] Equal contribution
[#]Current address, Section of Molecular Biology, Division of Biological Sciences, University of California San Diego, La Jolla, CA

Abstract

The canonical mechanism of microtubule-based movement uses adaptor proteins to link cargos to the molecular motors dynein and kinesin. Recently, an alternative mechanism known as "hitchhiking" was discovered: ribonucleoproteins, peroxisomes, lipid droplets, and endoplasmic reticulum achieve motility by hitching a ride on motile early endosomes, rather than attaching directly to a motor protein. In the filamentous fungus *Aspergillus nidulans* we identified a molecular linker, PxdA, that associates with early endosomes and is essential for peroxisome hitchhiking. However, the molecular components that interact with PxdA, as well as the regulatory mechanisms that govern hitchhiking, are not understood. Here, we report the identification of two new *pxdA* alleles, including a point mutation (R2044P). We find that the R2044P mutation disrupts PxdA's ability to associate with early endosomes and consequently reduces peroxisome movement. We also identify the phosphatase DipA as an interaction partner of PxdA. DipA associates with early endosomes in a PxdA-dependent manner, and regulates the movement and distribution of peroxisomes. Finally, we find that PxdA also regulates the distribution of lipid droplets, but not autophagosomes or mitochondria. Our data suggest that PxdA is a central regulator of early endosome-dependent hitchhiking and requires the DipA phosphatase to regulate the movement and distribution of lipid droplets and peroxisomes.

Keywords: hitchhiking, endosome, peroxisome, lipid droplet, dynein, kinesin

Introduction

The precise spatiotemporal distribution of cargos is critical for cell growth, maturation, and maintenance. Long-distance movement of cargos including vesicles, organelles, mRNAs, and macromolecular complexes is driven by molecular motor-dependent transport on microtubules [1-3]. Microtubules are polarized structures with their "plus" ends located near the cell periphery and "minus" ends embedded near the nucleus at microtubule-organizing centers. In mammalian cells, dozens of kinesin motors carry cargos long distances towards the cell periphery, but a single cytoplasmic-dynein-1 ('dynein' here) transports cargos towards the cell center [1, 2, 4].

The filamentous fungus *Aspergillus nidulans* is an ideal model system to study mechanisms of microtubule-based transport [5, 6]. Similar to mammalian cells, but unlike budding yeast, *A. nidulans* uses microtubule-based transport for the distribution and long-distance movement of cargos. It encodes one dynein, *nudA*, and three cargo-carrying kinesins including a kinesin-1, *kinA* and two kinesin-3's, *uncA* and *uncB* [5, 6]. Methods for live-cell imaging in *A. nidulans* are well-established and the microtubules near the hyphal tip are uniformly polarized with their plus ends oriented outward, making the directionality of cargo transport and the motors involved easy to identify. We and others have exploited these features by performing forward genetic screens to identify regulators of microtubule-based transport [7-14].

The current dogma of microtubule-based transport is that distinct cargos directly recruit molecular motors via adaptors [1, 15-17]. For example, in mammalian cells, members of the Bicaudal-D and Hook cargo adaptor families link dynein and kinesins to cargo [18-28]. Altogether, there are dozens of cargo adaptors from at least three diverse protein families in mammals [1]. On the other hand there are relatively few in filamentous fungi, the primary cargo adaptor being a homologue from the Hook family (HookA in *Aspergillus nidulans* and Hok1 in *Ustilago maydis*) [9, 29]. Hook is one part of the FHF complex, composed of Fts, Hook, and Fts-Hook-Interacting Protein (FHIP), which is thought to link dynein (and kinesin-3 in some instances) to early endosomes (EEs) via the small GTPase Rab5 [10, 29-31]. In both *A. nidulans* and *U. maydis*, EEs are the best-characterized cargo that has been shown to link to dynein and kinesin [32-35]. However, many cargos are properly distributed along the hyphal axis in *A. nidulans* and *U. maydis*. How these fungi are capable of properly distributing many cargos despite few genetically encoded motors and adaptors remains an unresolved question. Recently, a non-canonical mechanism of transport termed 'hitchhiking' was discovered [36-40]. A hitchhiking cargo, rather than connecting directly to an adaptor-motor complex, instead achieves motility by attaching itself to an already-motile cargo [41]. Via hitchhiking, many cargos can be evenly distributed throughout a cell by attaching and detaching from a single motor-bound cargo, making hitchhiking an ideal form of transport for organisms with few genetically-encoded motors [42, 43].

A number of cargos have been shown to exhibit hitchhiking-like behaviors in different organisms and contexts. In budding yeast,

mammalian neurons, and *U. maydis*, mRNAs are tethered to and co-transported with different membrane-bound compartments [44-48]. In *U. maydis*, polysomes associate with the RNA-binding protein Rrm4, which interacts with the EE-associated protein Upa1 [36-38, 49]. In neurons, ANXA11 links RNA granules to lysosomes [44]. Membrane-bound organelles, including peroxisomes, also hitchhike on highly motile EEs in both *U. maydis* and *A. nidulans* [39, 40]. Though no linkers have been identified in *U. maydis* [50], a mutagenesis screen in *A. nidulans* revealed the protein PxdA as a critical mediator of peroxisome hitchhiking [39]. However, how PxdA links peroxisomes to EEs and whether other proteins are involved remain unclear. In *U. maydis,* lipid droplets and the endoplasmic reticulum also hitchhike on EEs [40]. Whether PxdA mediates hitchhiking of these or other organelles in *A. nidulans* remains to be determined.

In this study, we sought to investigate new modes of regulation of hitchhiking in *A. nidulans*. We took a three-pronged approach: First, we returned to the initial screen that identified PxdA and identified two new *pxdA* alleles, one of which is a point mutation (R2044P) that inhibits the association of PxdA with EEs. Second, we used immunoprecipitation mass spectrometry to identify PxdA interactors and identified the DenA/Den1 phosphatase DipA. DipA is recruited to EEs in a PxdA-dependent manner and is required for peroxisome motility. Third, we screened other organelles including mitochondria, autophagosomes, and lipid droplets to determine whether PxdA was required for the proper distribution of other intracellular cargos. We found that lipid droplet distribution was perturbed in *pxdAΔ* hyphae, suggesting a broader role for PxdA in regulating hitchhiking of other cargos in the cell.

Results

Identification of novel pxdA alleles

In a previous screen to identify novel regulators of microtubule-based transport, we mutagenized an *A. nidulans* strain expressing three fluorescently-labeled organelles known to be distributed by dynein and kinesin: EEs (GFP-RabA/5a), peroxisomes (peroxisome targeting signal mCherry-PTS1), and nuclei (Histone H1, HH1-BFP) [8]. From this screen, we identified two mutants with peroxisome-specific defects that mapped to two independent alleles in the gene *AN1156/pxdA,* which led to early stop codons ($PxdA_{S201stop}$ and $PxdA_{Q846stop}$) in the protein (Figure 1A) [39]. PxdA has a long uncharacterized region (UR1) at its amino-terminus followed by a ~600 a.a. coiled coil (CC) region comprised of three tandem coiled coils (CC1, CC2 and CC3) and a shorter uncharacterized region (UR2) at its carboxy-terminus (Figure 1A). We previously determined that the CC2 and CC3 domains were necessary for association with EEs, while the region containing CC1, CC2 and CC3 was sufficient for association with EEs [39].

Here, we sought to identify other regulators of peroxisome hitchhiking. We first returned to our initial screen that identified PxdA [8, 39]. We sequenced additional mutants with peroxisome-specific defects and identified two new *pxdA* alleles. One of these alleles created a stop codon at Q1201 ($PxdA_{Q1201stop}$; Figure 1A). The other allele, R2044P was located in the CC3 domain of PxdA ($PxdA_{R2044P}$; Figure 1A). Both new alleles showed defects in peroxisome motility, but had normal EE motility and nuclear distribution (Figure 1, B-E). We chose to focus on the $pxdA_{R2044P}$ allele.

A point mutation in PxdA decreases its ability to associate with early endosomes

As the R2044P mutation is present within the CC3 domain, and the CC2 and CC3 domains are required for association of PxdA with EEs [39], we hypothesized that this mutation would affect the ability of PxdA to

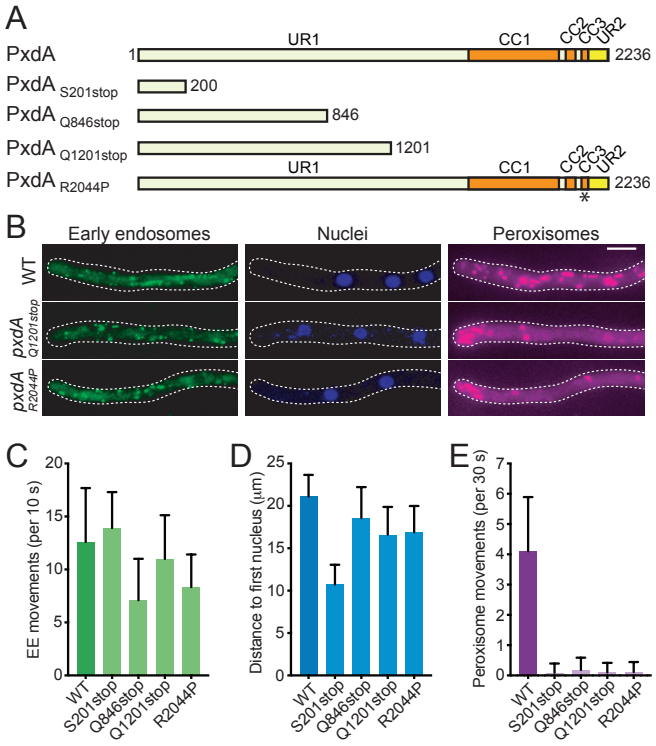

Figure 1 – Novel *pxdA* alleles regulate peroxisome movement and distribution. (A) Schematic of PxdA domain organization and novel PxdA mutants. $PxdA_{S201stop}$, $PxdA_{Q846stop}$, and $PxdA_{Q1201stop}$ mutations create stop codons that result in truncated proteins, while the $PxdA_{R2044P}$ point mutation is in the CC3 domain of PxdA (indicated by an asterisk). **(B)** Representative images of the distribution of peroxisomes (mCherry-PTS1), nuclei (HH1-BFP) and EEs (GFP-RabA) in wild-type (WT), $pxdA_{Q1201stop}$, and $pxdA_{R2044P}$ hyphae. **(C-E)** Quantification of movement of EEs (C), distribution of nuclei (D), and movement of peroxisomes (E) in $pxdA_{Q1201stop}$ and $pxdA_{R2044P}$ hyphae compared to previously identified *pxdA* alleles [8, 39]. EE and peroxisome movement is quantified as the number of EEs or peroxisomes crossing a line drawn perpendicular and 10 µm away from the hyphal tip during a 10- or 30-sec time-lapse video, respectively. Data is mean ± SD. n = 10 (WT), 11 ($pxdA_{Q846stop}$),11 ($pxdA_{S201stop}$), 10 ($pxdA_{Q1201stop}$), 9 ($pxdA_{R2044P}$) hyphae. *p < 0.05, ****p < 0.0001 (Krustal-Wallis test with Dunn's multiple comparisons test compared to wild-type strain).

associate with EEs. To test this, we created a fluorescently-tagged version of $PxdA_{R2044P}$ at the endogenous *pxdA* locus. Replacement of endogenous PxdA with $PxdA_{R2044P}$-mTagGFP2 ($PxdA_{R2044P}$-GFP) resulted in a significant decrease in peroxisome motility compared to a strain expressing wild-type PxdA-GFP (Figure 2A and Video 1). However, this decrease in peroxisome motility was not as substantial as in a *pxdAΔ* strain (Figure 2A). We then examined the localization and dynamics of $PxdA_{R2044P}$-GFP compared to wild-type PxdA-GFP. $PxdA_{R2044P}$-GFP showed a more diffuse localization, with few moving foci (Figure 2B, and Video 2), suggesting a defect in associating with EEs. Supporting this, we found that while many wild-type PxdA-GFP runs colocalized with EEs, there was little colocalization between $PxdA_{R2044P}$-GFP and EEs (Figure 2, C and D). EEs moved normally in this strain. Together, these findings demonstrate that a single mutation in the CC3 domain of PxdA is capable of disrupting PxdA's association with EEs, resulting in decreased peroxisome hitchhiking.

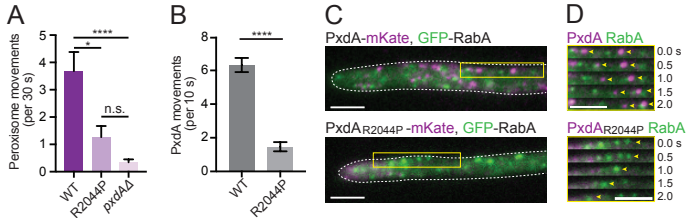

Figure 2 – A point mutation in the CC3 domain of PxdA decreases PxdA association with early endosomes. (A) Bar graphs of peroxisome movements in wild-type (WT), *pxdA*$_{R044P}$, and *pxdA*Δ hyphae, quantified as the number of peroxisomes crossing a line drawn perpendicular and 10 µm away from the hyphal tip during a 30-sec time-lapse video. Data is mean ± SEM. n = 22 (WT), 27 (PxdA$_{R044P}$), and 38 (*pxdA*Δ) hyphae. *p = 0.114, ****p < 0.0001 by Krustal-Wallis test with Dunn's multiple comparisons test. Also see Video 1. **(B)** Bar graphs of PxdA(WT)-mTagGFP2 and PxdA$_{R044P}$-mTagGFP2 movements quantified as the number of PxdA puncta crossing a line drawn perpendicular and 10 µm away from the hyphal tip during a 10-sec time-lapse video. Data is mean ± SEM. n = 17 (WT), 17 (PxdA$_{R044P}$) hyphae. ****p < 0.0001 (Mann Whitney test). Also see Video 2. **(C)** Representative images of hyphae expressing mTagGFP2-RabA (GFP-RabA) and wild-type PxdA-mKate or PxdA$_{R044P}$-mKate. Scale bar, 5 µm. **(D)** Representative time-lapse stills from region indicated by yellow box in (C), demonstrating co-localization of EEs (GFP-RabA) with wild-type PxdA, but not PxdA$_{R044P}$. Yellow arrowheads denote moving EEs (GFP-RabA). Scale bars, 5 µm.

PxdA interacts with the DipA phosphatase on EEs

Our mutagenesis screen identified 4 alleles of *pxdA*, but no additional genes involved in hitchhiking. To identify other proteins that might be involved in hitchhiking, we immunoprecipitated PxdA and identified interacting proteins using mass spectrometry. Specifically, lysates from hemagglutinin (HA)-tagged PxdA and untagged wild-type strains were immunoprecipitated with HA-conjugated agarose. PxdA resolves at approximately 250 kilodaltons on SDS-PAGE gels when lysates are prepared under denaturing conditions [39]. However, when lysates are prepared under non-denaturing conditions PxdA is partially degraded (Figure 3A, left panel). Despite this degradation, we could detect an additional faster migrating band (between 75-100 kDa) by Sypro stain (Figure 3A, right panel) that was present in the HA immunoprecipitations and not present in the control. Mass spectrometry analysis revealed this band to be the *D*enA/DEN1 *i*nteracting *p*hosphatase (DipA). DipA interacts with and regulates the stability of the deneddylase DenA/DEN1 on motile puncta in the cytoplasm, a process important for fungal asexual development [51].

We next sought to determine where DipA is localized, how it interacts with PxdA, and whether it regulates peroxisome movement. To accomplish this, we constructed two DipA strains: (1) an endogenously tagged DipA with two tandem copies of TagGFP2 at its carboxy-terminus (DipA-GFP) to assess its localization, and (2) a DipA deletion (*dipA*Δ) strain to assess its cellular function. As previously reported, the *dipA*Δ strain exhibits perturbed colony growth (Supplementary Figure 1A) [51]. Colonies from the DipA-GFP strain grow normally (Supplementary Figure 1A), suggesting that the GFP tag does not adversely affect protein function. We performed live-cell imaging of DipA-GFP and found that DipA localizes to highly motile puncta (Figure 3B, and Video 3) that have a similar velocity to PxdA puncta and EEs (Figure 3C) [33, 39, 52]. Consistent with this, the vast majority of motile DipA puncta colocalize with PxdA (Figure 3, D-F). Furthermore, in a *hookAΔ* strain in which EEs accumulate in the hyphal tip [9], DipA displays similar accumulation (Figure 3, G and H), suggesting that DipA associates with EEs along with PxdA.

Since PxdA and DipA interact and colocalize on the same motile EEs, we wondered if PxdA required DipA for its localization or vice versa. To test this, we first imaged the dynamics of PxdA in the absence of DipA (*dipA*Δ). We find that PxdA displays similar localization (Figure 4A) and motility in wild-type versus *dipA*Δ cells (Figure 4, B and C and Video 4). In contrast, we find that DipA is largely cytosolic in *pxdA*Δ hyphae (Figure 4D) and exhibits no detectable long-range movement (Figure 4, E and F and Video 5). Importantly, there are no differences in DipA protein expression levels in *pxdA*Δ vs wild-type strains (Supplementary Figure 1C). These results suggest that PxdA is required for the recruitment of DipA to EEs.

DipA regulates peroxisome movement

Based on our observations thus far, we hypothesized that DipA is required for peroxisomes to hitchhike on moving EEs. To test this, we examined peroxisome and EE distribution in a *dipA*Δ strain. Similar to *pxdA*Δ hyphae [39], *dipA*Δ hyphae displayed abnormal accumulation of peroxisomes near the hyphal tip (Figure 5, A and B), while EEs were distributed normally (Figure 5, C and D). The *dipA*Δ strain also showed a drastic reduction in peroxisome movement, but normal movement of EEs (Figure 5, E and F, and Videos 6 and 7). Therefore, the *dipA*Δ strain

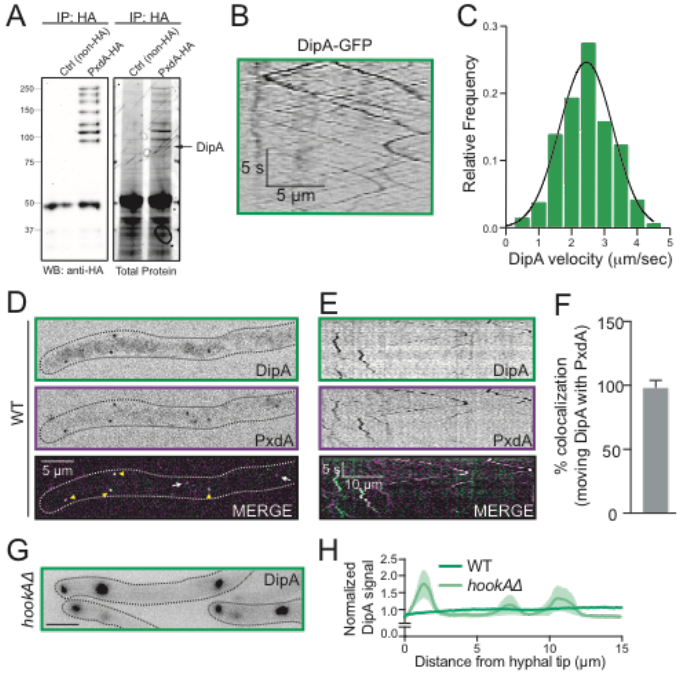

Figure 3. DipA associates with PxdA-marked endosomes. (A) Sypro Ruby-stained SDS-PAGE gel of lysates incubated with HA-conjugated agarose from wild-type (Ctrl) or PxdA-HA expressing hyphae. Mass spectrometry identified DipA (indicated by arrow) from two biological replicates. **(B)** Representative kymograph of DipA-GFP movement. Also see Video 3. **(C)** Histogram of DipA-GFP velocities calculated from kymographs as in (B). Mean velocities are 2.44 ± 0.77 (SD) µm/sec. n = 257 moving events. **(D)** Colocalization of DipA-GFP and PxdA-mKate along a hypha. **(E)** Representative kymograph of DipA and PxdA co-movement. **(F)** Quantification of the percent overlap of DipA colocalized with PxdA. Mean percent overlap is 97.88 ± 6.01 (SD). N = 8 kymographs. **(G)** Representative image of DipA-GFP distribution in *hookAΔ* hyphae. **(H)** DipA-GFP distribution is quantified by fluorescence intensity line-scans of fluorescently-tagged organelles in wild-type (WT) or *hookAΔ* hyphae. Mean fluorescence intensity (solid lines) ± SEM (shading) is plotted as a function of distance from the hyphal tip. n = 3 (WT) and 7 (*hookAΔ*) hyphae.

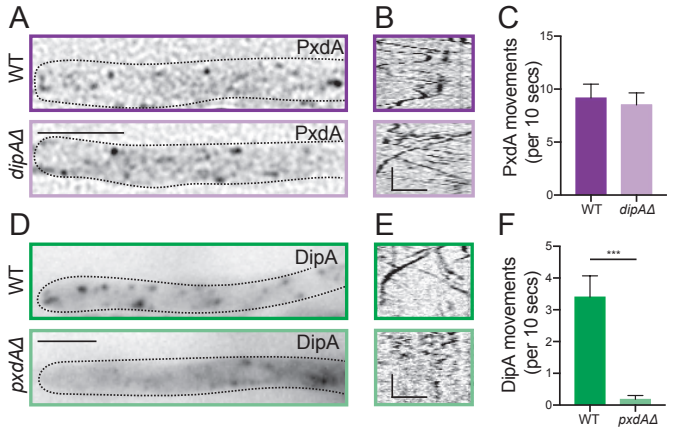

Figure 4. PxdA is required for DipA localization on moving foci (A) Representative micrograph demonstrating normal distribution of PxdA-GFP puncta along a hypha from a *dipA*Δ strain. Scale bar, 5 µm. **(B)** Representative kymograph of PxdA movement in a wild-type (WT; top) or *dipA*Δ (bottom) background. Scale bars, 2.5 µm (horizontal), 5 s (vertical). Also see Video 4. **(C)** Bar graph of the flux of PxdA movements in wild-type and *dipA*Δ hyphae calculated as the number of PxdA foci crossing a line drawn perpendicular and 10 µm away. **(D)** Representative micrograph demonstrating a primarily diffuse signal of DipA-GFP along a hypha in a *pxdA*Δ strain compared to wild-type. Scale bar, 5 µm. **(E)** Representative kymograph of DipA movement in a wild-type (top) or *pxdA*Δ (bottom) background. Scale bars, 2.5 µm (horizontal), 5 s (vertical). Also see Video 5. **(F)** Bar graph of the flux of PxdA movements in wild-type and *dipA*Δ hyphae calculated as the number of PxdA foci crossing a line drawn perpendicular and 10 µm away. n = 25 (WT) and 11 (*dipA*Δ) hyphae. ***p = 0.0002 (Mann Whitney test).

phenocopies the *pxdA*Δ strain, consistent with our observation that both proteins associate with the same subset of EEs.

During peroxisome hitchhiking, PxdA-labeled EEs colocalize at the leading edge of moving peroxisomes [39, 40], suggesting that PxdA and EEs might dictate the directionality of moving peroxisomes. We were curious if moving DipA foci interacted with peroxisomes in a similar manner. We first monitored the flux of peroxisomes in the DipA-GFP strain and found that tagging DipA does not perturb peroxisome movement (Supplementary Figure 1B). Next, using simultaneous two-color imaging of DipA and peroxisomes, we found that motile DipA localizes to the leading edge of peroxisomes (Figure 5, G and H), similar to our previously published data on PxdA [39]. In further support of this, DipA shifts to the leading edge of peroxisomes concurrent with rapid directional switches in peroxisome movement (Figure 5G and Video 8). In summary, we find that DipA localizes to PxdA-labeled EEs and is critical for peroxisome hitchhiking.

Proper lipid droplet distribution requires PxdA

We next sought to determine whether the proper distribution of other organelles in *A. nidulans* hyphae required PxdA. To do this, we fluorescently tagged autophagosomes (GFP-Atg8), mitochondria (Tom20-GFP), and lipid droplets (AN7146-mKate) in wild-type and *pxdA*Δ cells. To quantify organelle distribution, we generated line scans along hyphae and quantified their fluorescence intensity. Autophagosomes and mitochondria showed similar fluorescent intensity profiles in wild-type and *pxdA*Δ hyphae (Figure 6, A and B). However, lipid droplets showed an altered fluorescently intensity profile in *pxdA*Δ hyphae, with an accumulation of lipid droplets observed ~15-20 µm from the hyphal tip (Figure 6C, asterisk), typically the site of the nucleus [8]. This data suggest that PxdA is also involved in lipid droplet distribution in *A. nidulans*. Together, our results identify novel regulators of peroxisome and lipid droplet hitchhiking

Discussion

Proper cargo transport is critical for many cell types, including filamentous fungi, in which cellular cargos are evenly distributed along their hyphae. Hitchhiking is a mode of transport whereby one type of cargo achieves motility via attachment to another type of motile cargo. We previously found that the protein PxdA is required for peroxisomes to hitchhike on EEs in *A. nidulans.* In this study, we identified two novel mutant alleles of PxdA, including a single residue mutation ($PxdA_{R2044P}$) that disrupts PxdA association with EEs. We also identified a novel regulator of peroxisome hitchhiking, the phosphatase DipA. We found that DipA is required for peroxisome motility, colocalizes with PxdA, and its EE association requires PxdA. Finally, we found that PxdA is required for the proper distribution of lipid droplets, but not mitochondria or autophagosomes. Together, these data provide further insight into factors that affect organelle hitchhiking in *A. nidulans.*

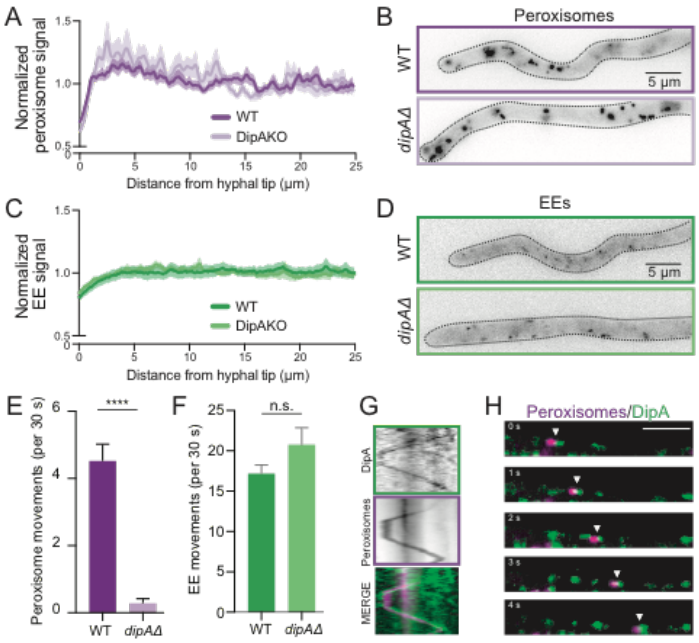

Figure 5. DipA regulates the movement and distribution of peroxisomes. (A) Distribution of peroxisomes along wild-type and *dipA*Δ hyphae. Data is normalized mean intensity ± SEM. n = 22 (WT) and 20 (*dipA*Δ) hyphae. Distribution comparing genotypes is significant ($p < 0.0001$) by two-way ANOVA. **(B)** Representative micrographs of peroxisomes along wild-type (WT) and *dipA*Δ hyphae. **(C)** Distribution of EEs along wild-type and *dipA*Δ hyphae. n = 7 (WT) and 6 (*dipA*Δ) hyphae. Distribution comparing genotypes is not significant by two-way ANOVA. **(D)** Representative micrographs of EEs along wild-type and *dipA*Δ hyphae. **(E)** Bar graph of the flux of peroxisome movements in wild-type and *dipA*Δ hyphae calculated as the number of peroxisomes crossing a line drawn perpendicular and 10 µm away. ****$p < 0.0001$, Mann-Whitney test. Also see Video 6. **(F)** Bar graph of flux of EE movements in wild-type and *dipA*Δ hyphae calculated as in (A). n = 17 (WT) and 16 (*dipA*Δ) hyphae. Also see Video 7. **(G-H)** Kymographs (E) and time-lapse stills (F) demonstrating colocalization of DipA-GFP with moving peroxisomes. Also see Video 8.

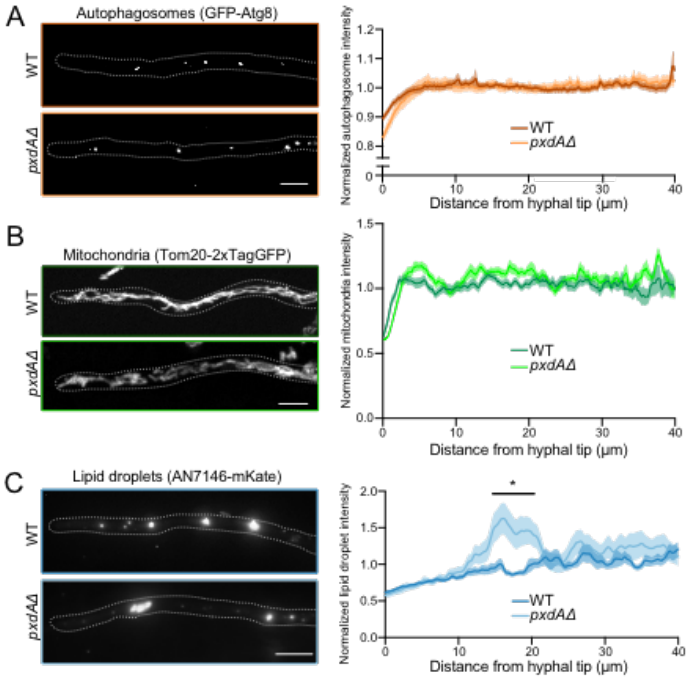

Figure 6. PxdA regulates the distribution of lipid droplets but not autophagosomes or mitochondria. (A-C, left panels) Representative micrographs of wild-type (WT) or *pxdAΔ* hyphae with fluorescently tagged autophagosomes (GFP-Atg8) (A), mitochondria (Tom20-GFP) (B), or lipid droplets (AN7146-mKate) (C). Scale bars, 5 μm. **(A-C, right panels)** Organelle distribution is quantified by fluorescence intensity line-scans of fluorescently-tagged organelles in wild-type or *pxdAΔ* hyphae. Mean fluorescence intensity (solid lines) ± SEM (shading) is plotted as a function of distance from the hyphal tip. For autophagosomes, n = 23 (WT) and 23 (*pxdAΔ*) hyphae from 2 replicates. For mitochondria, n = 37 (WT) and 31 (*pxdAΔ*) hyphae from 3 replicates. For lipid droplets, n = 37 (WT) and 34 (*pxdAΔ*) hyphae from 3 replicates. Lipid droplet distribution was significantly different (*$p < 0.05$) between wild-type and *pxdAΔ* hyphae (two-way ANOVA, Sidak's multiple comparisons test significant between 15 and 19 μm from the hyphal tip).

A single residue mutation in PxdA decreases its association with early endosomes

We previously showed that the CC2 and CC3 domains of PxdA are required for its association with EEs [39]. We found that a PxdA mutant allele (*pxdA$_{R2044P}$*) disrupts PxdA association with EEs via a single amino acid change in CC3. This mutation may disrupt PxdA's ability to interact with a binding partner on the EE surface or with the EE membrane directly. The PxdA$_{R2044P}$ mutant will be an important tool in the future to characterize how PxdA associates with EEs and whether PxdA directly or indirectly links EEs to hitchhiking cargos.

DipA is a regulator of peroxisome hitchhiking

Our proteomics experiments identified the phosphatase DipA as a PxdA interactor. DipA associates with the PxdA-bound population of EEs and is required for peroxisomes to hitchhike on EEs. DipA requires PxdA to associate with EEs. DipA is a phosphatase whose function was previously linked to regulating the phosphorylation status and degradation of DenA/Den1, a protein involved in asexual spore formation [51, 53]. DenA is co-transported with DipA [51]. Given the similar co-transport of both DenA and PxdA with DipA, it is possible that DipA also regulates PxdA by modulating PxdA's phosphorylation state, allowing PxdA to differentially bind cargos in different circumstances. Future work will determine whether PxdA is phosphorylated and whether its phosphorylation state is regulated by DipA.

Though we do not understand how the PxdA-DipA complex links to peroxisomes, it is also possible that DipA regulates the phosphorylation state of other proteins in the hitchhiking machinery, such as peroxisome-associated proteins. Alternatively, DipA may not regulate the phosphorylation state of the hitchhiking machinery, but may instead link PxdA to peroxisomes. Whether DipA links PxdA to peroxisomes or whether DipA regulates hitchhiking in other ways remains to be determined. Additionally, though DipA is required for peroxisome motility, whether DipA also affects the hitchhiking of lipid droplets or factors involved in lipid droplet biogenesis remains to be determined.

PxdA is required for proper lipid droplet distribution

Finally, we found that deleting PxdA affects lipid droplet distribution. Normally, lipid droplets are distributed evenly along hyphae. However, in *pxdA*Δ hyphae, lipid droplets accumulate ~15-20 μm from the hyphal tip—a region that generally corresponds to the first nucleus closest to the hyphal tip [8]. In *A. nidulans* hyphae, microtubules are uniformly polarized between the hyphal tip and the closest nucleus, with microtubule plus ends near the hyphal tip and microtubule minus ends near the first nucleus [5]. Therefore, dynein transport defects generally result in cargo accumulation near the hyphal tip, while kinesin-3/UncA transport defects result in cargo accumulation at the first nucleus. Interestingly, we observe that knocking out or mutating *pxdA* results in peroxisome accumulation at the hyphal tip (Figure 1B) [39], but lipid droplet accumulation at a region near the first nucleus (Figure 6C).

We favor a model whereby PxdA mediates peroxisome/lipid droplet transport in both directions (via linking these cargos to EEs). Thus, the location of organelle accumulation in *pxdAΔ* hyphae is dictated by the site of biogenesis of that organelle. In the filamentous fungus *Penicillium chrysogenum*, peroxisome biogenesis occurs preferentially at the hyphal tip [54]. If peroxisomes are also generated preferentially at the hyphal tip in *A. nidulans*, then a defect in transport in both directions would result in peroxisome accumulation at the hyphal tip. The sites of lipid droplet biogenesis in filamentous fungi are less clear. In other organisms, lipid droplet biogenesis occurs at privileged sites along the endoplasmic reticulum [55]. It is possible that lipid droplets or proteins required for lipid droplet biogenesis originate at endoplasmic reticulum sites near the nucleus, resulting in their accumulation near those sites in *pxdA*Δ hyphae. Therefore, disrupting the bidirectional hitchhiking function of PxdA could result in the accumulation of different organelles at different cellular locations. A final possibility is that actin-based 'polar drift' forces movement of peroxisomes toward the hyphal tip, as demonstrated in *Ustilago maydis* [43]. If this is also the case in *A. nidulans,* these forces must only affect peroxisomes, resulting in the accumulation of peroxisomes, but not lipid droplets, at the hyphal tip. Future work will be needed to identify additional regulators of lipid droplet distribution in *A. nidulans.* Together, our work identifies several modes of regulation of hitchhiking in *A. nidulans*.

Materials and Methods

Fungal growth conditions

A. nidulans strains were grown in yeast extract and glucose (YG) medium [56] or 1% glucose minimal medium [57], supplemented with 1 mg/ ml uracil, 2.4 mg/ ml uridine, 2.5 μg/ ml riboflavin, 1 μg/ml para-aminobenzoic acid, and 0.5 μg/ ml pyridoxine when required.

Glufosinate (Sigma) for *bar* selection was used at a final concentration of 700 µg/ mL.
For imaging of germlings, spores were resuspended in 0.5 mL 0.01% Tween-80 solution. The spore suspension was diluted at 1:1,000 in liquid minimal medium containing appropriate auxotrophic supplements. The spore and media mix (400 µL) was added to an eight-chambered Nunc Lab-Tek II coverglass (ThermoFisher) and incubated at 30°C for 16-20 hours before imaging. For imaging of mature hyphae, spores were inoculated on minimal medium plates containing the appropriate auxotrophic supplements and incubated at 37°C for 12-16 hours. Colonies were excised from agar plates and inverted on Lab-Tek plates for imaging. For biochemistry, spores were inoculated in YG medium containing the appropriate auxotrophic supplements for 16-20 hours at 37°C shaking at 200 rpm.

Plasmid and strain construction

Strains of *A. nidulans* used in this study are listed in Table S1. All strains were confirmed by a combination of PCR and/or sequencing from genomic DNA isolated as previously described [58] and in some cases by Western blot analysis. For all plasmids, PCR fragments were inserted into the Blue Heron Biotechnology pUC vector at 5' EcoRI and 3' HindIII restriction sites using Gibson isothermal assembly [59]. All plasmids were confirmed by Sanger sequencing. Initial strains were created by homologous recombination with linearized DNA to replace the endogenous gene in strains lacking *ku70 [57]* with *Afribo (Aspergillus fumigatus Ribo), AfpyrG* (*Aspergillus fumigatus pyrG*), or *Afpyro* (*Aspergillus fumigatus pyro*), or *bar* [60] as selectable markers. Additional strains were created using genetic crossing as previously described [61]. The strategies for transforming *hookA*Δ, *pxdA*Δ, PxdA-HA, PxdA-mTagGFP2, and PxdA-mKate2 strains, as well as the strains containing fluorescently labeled EEs, peroxisomes, and nuclei, have been previously described [8, 39]. The strategies for DNA constructs and strains created for the current study are as follows:

PxdA$_{R2044P}$-GFP/mKate. To construct this plasmid, carboxy-terminal codon-optimized fluorescent protein tags, either mTagGFP2 [62] or mKate2 [63] were preceded by a GA(x4) linker and followed by *AN1156*/*pxdA*'s native 3' UTR with flanking 1kb upstream and downstream homologous recombination arms. To introduce the Q2044P mutation, the upstream 1kb recombination arm was amplified by PCR from genomic DNA (gDNA) isolated from RPA568 (mutagenized strain harboring the Q2044P mutation) using the oligos 5'-GTCACGACGTTGTAAAACGACGGCCAGTGCCTTCAGGAGCGAGTGGCGCATCCGAAG-3' and 5'-CTGACATTGCACCTGCACCTGCACCTGCACCTGCTATTTGTGGGCCAAAGGGACCGTCGG-3'. To amplify the linearized DNA used for targeting via transformation, the oligos 5'-CCTTCAGGAGCGAGTGGCGCATCTC-3' and 5'-GACGTTGACACTTCGTGCTAGAACT-3' were used.

GFP-PxdA. This N-terminal GFP-tagged PxdA construct was used for data collected in Figure 4, A and B. For ease of cloning, this construct lacks the first 816 aa of PxdA (PxdA$_{(\Delta 1\text{-}816)}$ starts with 5'-CAGCAGGTCCCGGTTCCAC-3' for reference), but is functional since it has no effect on peroxisome motility and distribution (data not shown) [39]. Codon-optimized mTagGFP2 with a GA(x4) linker was followed by the PxdA$_{(\Delta 1\text{-}816)}$ fragment (4260 bp), its native 3' UTR and an *AfpyrG* cassette, and flanked by 1kb homologous recombination arms. To amplify the linearized DNA used for transformations, the oligos 5'-AGTCGACACGGAAGGTTGGTCAATC-3' and 5'-GACGTTGACACTTCGTGCTAGAACT-3' were used. To identify positive clones with better efficiency, we targeted the linear PxdA$_{(\Delta 1\text{-}816)}$-*AfpyrG*-containing DNA into a *pxdA*Δ strain (RPA921) where the endogenous *pxdA* locus was replaced with *Afribo.* Using this strategy we positively selected clones that (1) grow on minimal media plates lacking supplemented uradine-uracil and (2) are unable to grow on plates lacking riboflavin. From there, we sequenced verified this strain and used genetic crosses to generate additional strains.

*dipA*Δ. This strain was originally previously published elsewhere [51], but it was remade for this study using a different strategy. Linearized DNA used for targeting was amplified with 5'-ATGAGACGAACCTGGCCATCAAGGC-3' and 5'-TTATGCCATGTTGCAGGTGGAA CA-3' by fusion PCR with fragments for a selectable marker flanked by upstream and downstream homologous recombination arms around the *AN10946/dipA* genomic locus.

DipA-GFP. A tandem 2x-mTagGFP2 preceded by a GA(x4) linker and followed by *AN10946/dipA*'s native 3' UTR with flanking 1kb upstream and downstream homologous recombination arms. This plasmid was digested with the Pci restriction enzyme (cut sites in the 5' and 3' homologous arms) to linearize DNA for targeting.

AN7146-mKate (lipid droplets). To visualize endogenously-labeled lipid droplets, we fluorescently tagged AN7146 (a putative S-adenosyl-methionine delta-24-sterol-C-methyltransferase). AN7146 is a homolog of Erg6 in *Ustilago maydis* and used as a lipid droplet marker in a previous study [40]. To create this plasmid, C-terminal codon-optimized mKate2 [63] was preceded by a GA(x4) linker and followed by *AN7146*'s native 3' UTR with flanking 1kb upstream and downstream homologous recombination arms. The oligos 5'-GTTGTTCAAAACCCTTGGGAAATTTG-3' and 5'-TCCAGTTGAAGTACACTACACATTCG-3' were used to amplify the linearized DNA fragment used for targeting.

GFP-AtgH (autophagosomes). To visualize autophagosomes, we fluorescently tagged the functional homolog of Atg8, *atgH/AN5131*. To construct this plasmid, the codon-optimized mTagGFP2 followed by a GA5 linker and the entire *atgH* locus (including its native 3'UTR) was flanked by homologous recombination arms. The oligos 5'-CTGTAAATTCTTTCTTGCCC-3' and 5'-CTTTGCCGTCGTATCGACC-3' were used to PCR amplify the targeting construct used for transformation.

Tom20-GFP (mitochondria). To visualize mitochondria, we fluorescently tagged the mitochondrial outer membrane component Tom20, *AN0559* [64]. To construct this plasmid, a codon-optimized 2xmTagGFP2 was preceded by a GSGSG linker and followed by *AN0559*'s native 3' UTR with flanking 1kb upstream and downstream homologous recombination arms. The oligos 5'-GGGCGGCGATTTTTGCTGCGAAGAG-3' and 5'-CGGATTTGCCGTCAACGGCGTTGGT-3' were used to amplify the linearized DNA fragment used for targeting.

Whole-genome sequencing

The general workflow for whole genome sequencing has been previously described [8]. The mutagenized strains, RPA568 and RPA639, were backcrossed to the parental RPA520 strain while tracking the presence of the peroxisome accumulation and motility phenotypes in order to (1) reduce the number of background mutations and (2) to ensure the phenotype likely arose from a single gene (see [8] for more details). Genomic DNA (gDNA) was prepared from a pool of at least five individual backcrossed strains and treated with RNase prior to a final

cleanup by phenol/chloroform extraction. gDNA was sheared with the Covaris S2 sonicator, and samples were run on a D1000 Tapestation to evaluate shearing success. Samples were normalized to the same input and prepped using KAPA HTP Library Prep Reagents using an Apollo 324 robot. This involved End-Repair, A-Tailing, and Adapter Ligation, followed by amplification and barcoding (similar to [8]). A bead-based cleanup removed primer-dimers and adapter-dimers. The final library products were run on a High Sensitivity D1000 Screentape and qPCR was performed using the KAPA Library Quantification kit. The libraries were then pooled and loaded onto an individual lane of the HiSeq 2500 Rapid flowcell, with a read length of ~50 base pairs. Data sets were sorted by barcode using Python software as previously described and the data were aligned using the *A. nidulans* reference genome FGSC_A4. Genomic data was sorted for genomic feature (i.e. exon, intron) and mined specifically at the *AN1156/pxdA* locus for high quality (> 5 times in the mutant data set and zero in the backcrossed wild-type mutagenized strain) and uncommon (i.e., not in the wild-type backcrossed strain) nonsynonymous mutations.

Imaging acquisition

All images were collected at room temperature. All flux and line-scan measurements were acquired using an inverted microscope (Nikon, Ti-E Eclipse) equipped with a 60x and 100x 1.49 N.A. oil immersion objective (Nikon, Plano Apo), and a MLC400B laser launch (Agilent), with 405 nm, 488 nm, 561 nm and 640 nm laser lines. Excitation and emission paths were filtered using single bandpass filter cubes (Chroma). For two-color colocalization imaging in Figure 2, the emission signals were further filtered and split using W-view Gemini image splitting optics (Hamamatsu). Emitted signals were detected with an electron multiplying CCD camera (Andor Technology, iXon Ultra 888). Illumination and image acquisition were controlled with NIS Elements Advanced Research software (Nikon), and the xy position of the stage was controlled with a ProScan linear motor stage controller (Prior). Simultaneous two-color time-lapse images in Figs. 3 and Figure 5 were collected using a Plan Apo TIRF 60x/1.49 oil immersion objective on the Deltavision OMX Blaze V4 system (GE Healthcare). GFP and mKate2/mCherry were excited simultaneously with 488nm and 568nm diode laser lines, respectively. A BGR polychroic mirror was used to split emission light from fluorophores to different PCO Edge sCMOS cameras. Emission filters in front of both cameras was used to select appropriate wavelengths (528/48 and 609/37 for GFP and mKate/mCherry, respectively). Images were aligned with OMX image registration using softWoRx software and some images were deconvolved for display using the enhanced ratio method.

Image and Data analysis

Line-scan distribution and flux measurements were calculated as previously reported [39]. For line-scan measurements, maximum-intensity projections of fluorescence micrographs and brightfield images (for hyphae) were obtained using ImageJ/FIJI (National Institutes of Health, Bethesda, MD). Brightfield images were traced starting from the hyphal tip, using the segmented line tool (line width 25), and traces were superimposed on the fluorescence micrographs to project the average fluorescence intensity. For normalization of line-scans, each condition's average immunofluorescence intensity values at each point along the hyphae were normalized against that condition's total baseline average. For flux measurements, the number of puncta crossing a line approximately 10 µm perpendicular to and from the hyphal tip was manually counted. All peroxisome flux data were calculated from 30-sec time-lapse videos, while all EE, DipA, and PxdA flux data were calculated from 10-sec time-lapse videos. DipA velocity (Figure 3D) was analyzed using ImageJ. Specifically, maximum-intensity projections were generated from time-lapse sequences to define the trajectory of particles of interest. The segmented line tool was used to trace the trajectories and map them onto the original video sequence, which was subsequently resliced to generate a kymograph. The instantaneous velocities of individual particles were calculated from the inverse of the slopes of kymograph traces. For distance to first nucleus measurements (Figure 1D), nuclei were thresholded in ImageJ and the segmented line tool was used to measure the distance from the hyphal tip to the edge of the first nucleus.

For DipA/PxdA colocalization measurements, DipA and PxdA kymographs were generated from simultaneous two-color time-lapse videos. DipA kymographs were thresholded in ImageJ, manually traced using the segmented line tools, and traces were then superimposed onto the PxdA kymograph to manually determine overlap. The fractional overlap (colocalization) of DipA with PxdA for each kymograph was calculated. Due to the weak and unreliable fluorescence signal of DipA in our time-lapse videos, we were unable to determine the fraction of PxdA that colocalized with DipA.

All statistical analyses were performed using Prism8 (GraphPad).

Cell Lysis and Immunoprecipitations

Overnight cultures for biochemistry were strained in miracloth (Millipore), flash frozen in liquid nitrogen, and ground with a mortar/pestle in the presence of liquid nitrogen. For Western blot expression analysis of DipA-GFP in wild-type and *pxdAΔ* strains (Figure 4G), 250 uL of packed ground mycelia were resuspended in 500 uL boiling denaturing buffer (125 mM Tris-HCl pH 6.8, 9M Urea, 1mM EDTA pH7.0, 4% SDS, 10mM DTT, 10% beta-ME, 4% glycerol), rotated for 10 mins at room temperature (RT), spun at 20,000 x g for 10 mins at RT, and followed by addition of 1x Laemmli buffer (BioRad) to the supernatant. For anti-HA immunoprecipitations from wild-type and PxdA-HA strains used for mass spectrometry analysis (Figure 3A), all steps were performed at 4°C unless otherwise stated. Approximately 4 mLs packed ground mycelia were lysed in 10 mLs of modified RIPA buffer (150 mM NaCl, 50 mM Tris pH 8.0, 1% Triton X-100, 0.1% SDS) supplemented with protease inhibitor cocktail (Roche). Lysates were rotated for 30 mins, and centrifuged for 5 mins at 1000 x g. Supernatants were subjected to two additional 20,000 x g spins for 20 mins each. Agarose beads were added to clarified supernatants and rotated over-end for 1 hr to pre-clear any non-specific interactions. Pre-cleared lysate was incubated with HA-conjugated agarose beads (ThermoFisher) and rotated over-end for 1.5 hrs. Beads were washed 3x with modified RIPA buffer and were subsequently boiled in Laemmli buffer for 5 mins prior to running on an SDS-PAGE gel.

Western blotting and mass spectrometry

All protein samples were resolved on 4-12% gradient SDS-PAGE gels (Life Technologies) for 60 mins. For Western blotting, gels were transferred to nitrocellulose for 3 hrs at 250 mA in 4°C. Blots were blocked with 5% milk in TBS-0.1% Tween-20 (TBS-T). Antibodies were diluted in 5% milk in TBS-T. Primary antibodies were incubated overnight at 4°C and horseradish peroxidase (HRP)-conjugated secondary antibodies (ThermoFisher) were incubated at RT for 1 hr. For DipA-2xmTagGFP expression (Figure 4G), rabbit anti-Tag(CGY)FP (Evrogen) was used at 1:2000. For PxdA-HA expression (Figure 3A), mouse anti-HA (Sigma) was used at 1:1000. Secondary antibodies were used at 1:10,000. Blots were rinsed 3x TBS-T for 10 mins after primary and secondary antibodies. Electrochemiluminescence was produced with

HRP and Prosignal Pico (Prometheus) detection reagent and imaged on a ChemiDoc (BioRad) using Image Lab (v5.2.1.) software.
For Sypro protein staining and subsequent mass spectrometry of anti-HA immunoprecipitations (Figure 3A), SDS-PAGE gel was incubated in Sypro Red protein gel stain (ThermoFisher) at 1:5000 in 7.5% acetic acid for 45 mins. Band of interest was excised and submitted to the Taplin Mass Spectrometry Facility at Harvard Medical School. A before and after picture using Sypro Ruby detection on the ChemiDoc (BioRad) was obtained to ensure the correct bands were excised. Excised gel bands were cut into approximately 1 mm^3 pieces. Gel pieces were then subjected to a modified in-gel trypsin digestion procedure [65]. Gel pieces were washed and dehydrated with acetonitrile for 10 min. followed by removal of acetonitrile. Pieces were then completely dried in a speed-vac. Rehydration of the gel pieces was with 50 mM ammonium bicarbonate solution containing 12.5 ng/µl modified sequencing-grade trypsin (Promega, Madison, WI) at 4ºC. After 45 min., the excess trypsin solution was removed and replaced with 50 mM ammonium bicarbonate solution to just cover the gel pieces. Samples were then placed in a 37ºC room overnight. Peptides were later extracted by removing the ammonium bicarbonate solution, followed by one wash with a solution containing 50% acetonitrile and 1% formic acid. The extracts were then dried in a speed-vac (~1 hr) and stored at 4ºC until analysis. On the day of analysis the samples were reconstituted in 5 - 10 µl of HPLC solvent A (2.5% acetonitrile, 0.1% formic acid). A nano-scale reverse-phase HPLC capillary column was created by packing 2.6 µm C18 spherical silica beads into a fused silica capillary (100 µm inner diameter x ~30 cm length) with a flame-drawn tip. After equilibrating the column each sample was loaded via a Famos auto sampler (LC Packings, San Francisco CA) onto the column. A gradient was formed and peptides were eluted with increasing concentrations of solvent B (97.5% acetonitrile, 0.1% formic acid). As peptides eluted they were subjected to electrospray ionization and then entered into an LTQ Orbitrap Velos Pro ion-trap mass spectrometer (Thermo Fisher Scientific, Waltham, MA). Peptides were detected, isolated, and fragmented to produce a tandem mass spectrum of specific fragment ions for each peptide. Peptide sequences (and hence protein identity) were determined by matching to the *A. nidulans* FGSC A4 protein database in Uniprot with the acquired fragmentation pattern by the software program, Sequest (Thermo Fisher Scientific, Waltham, MA). All databases include a reversed version of all the sequences and the data was filtered to between a one and two percent peptide false discovery rate.

Author Contributions and Notes

JS, JRC, and SLR-P devised the experiments. JS and JRC performed all experiments with help from AA-M. NS shared unpublished findings about DipA. SLR-P supervised the research. JS, JRC, and SLR-P wrote and edited the manuscript.

Acknowledgments

We thank Stephen A. Osmani for personal communication and sharing unpublished data on DipA. We also thank Thomas L. Schwarz for providing guidance and supervision of J.S. for part of this project. The Nikon Imaging Centers at Harvard Medical School and UC San Diego provided technical support and advice, and Ross Tamaino and the Taplin Mass Spectrometry Facility at Harvard Medical School provided technical support on mass spectrometry experiments. The Bioinformatics Department at the Harvard T.H. Chan School of Public Health assisted with whole genome sequencing data analysis. JS was funded for part of this work by the Charles King Trust Fellowship supported by the Charles H. Hood Foundation. JRC is funded by a postdoctoral fellowship from the National Institutes of Health (F32GM126692). SLR-P is an investigator of the Howard Hughes Medical institute and is also supported by R01GM121772.

References

1. Reck-Peterson, S.L., et al., *The cytoplasmic dynein transport machinery and its many cargoes.* Nat Rev Mol Cell Biol, 2018. **19**(6): p. 382-398.
2. Cianfrocco, M.A., et al., *Mechanism and Regulation of Cytoplasmic Dynein.* Annu Rev Cell Dev Biol, 2015. **31**: p. 83-108.
3. Vale, R.D., *The molecular motor toolbox for intracellular transport.* Cell, 2003. **112**(4): p. 467-80.
4. Hirokawa, N., et al., *Kinesin superfamily motor proteins and intracellular transport.* Nat Rev Mol Cell Biol, 2009. **10**(10): p. 682-96.
5. Egan, M.J., M.A. McClintock, and S.L. Reck-Peterson, *Microtubule-based transport in filamentous fungi.* Curr Opin Microbiol, 2012. **15**(6): p. 637-45.
6. Penalva, M.A., et al., *Searching for gold beyond mitosis: Mining intracellular membrane traffic in Aspergillus nidulans.* Cell Logist, 2012. **2**(1): p. 2-14.
7. Downes, D.J., et al., *Characterization of the Mutagenic Spectrum of 4-Nitroquinoline 1-Oxide (4-NQO) in Aspergillus nidulans by Whole Genome Sequencing.* G3 (Bethesda), 2014. **4**(12): p. 2483-92.
8. Tan, K., et al., *A microscopy-based screen employing multiplex genome sequencing identifies cargo-specific requirements for dynein velocity.* Mol Biol Cell, 2014. **25**(5): p. 669-78.
9. Zhang, J., et al., *HookA is a novel dynein-early endosome linker critical for cargo movement in vivo.* J Cell Biol, 2014. **204**(6): p. 1009-26.
10. Yao, X., X. Wang, and X. Xiang, *FHIP and FTS proteins are critical for dynein-mediated transport of early endosomes in Aspergillus.* Mol Biol Cell, 2014. **25**(14): p. 2181-9.
11. Yao, X., et al., *Discovery of a vezatin-like protein for dynein-mediated early endosome transport.* Mol Biol Cell, 2015. **26**(21): p. 3816-27.
12. Morris, N.R., *Mitotic mutants of Aspergillus nidulans.* Genet Res, 1975. **26**(3): p. 237-54.
13. Xiang, X., et al., *Isolation of a new set of Aspergillus nidulans mutants defective in nuclear migration.* Curr Genet, 1999. **35**(6): p. 626-30.
14. Xiang, X., S.M. Beckwith, and N.R. Morris, *Cytoplasmic dynein is involved in nuclear migration in Aspergillus nidulans.* Proc Natl Acad Sci U S A, 1994. **91**(6): p. 2100-4.
15. Cross, J.A. and M.P. Dodding, *Motor-cargo adaptors at the organelle-cytoskeleton interface.* Curr Opin Cell Biol, 2019. **59**: p. 16-23.
16. Fu, M.M. and E.L. Holzbaur, *Integrated regulation of motor-driven organelle transport by scaffolding proteins.* Trends Cell Biol, 2014. **24**(10): p. 564-74.
17. Olenick, M.A. and E.L.F. Holzbaur, *Dynein activators and adaptors at a glance.* J Cell Sci, 2019. **132**(6).
18. Matanis, T., et al., *Bicaudal-D regulates COPI-independent Golgi-ER transport by recruiting the dynein-dynactin motor complex.* Nat Cell Biol, 2002. **4**(12): p. 986-92.
19. Hoogenraad, C.C., et al., *Mammalian Golgi-associated Bicaudal-D2 functions in the dynein-dynactin pathway by interacting with these complexes.* EMBO J, 2001. **20**(15): p. 4041-54.
20. Hoogenraad, C.C. and A. Akhmanova, *Bicaudal D Family of Motor Adaptors: Linking Dynein Motility to Cargo Binding.* Trends Cell Biol, 2016. **26**(5): p. 327-40.
21. Schlager, M.A., et al., *Bicaudal d family adaptor proteins control the velocity of Dynein-based movements.* Cell Rep, 2014. **8**(5): p. 1248-56.
22. Schlager, M.A., et al., *In vitro reconstitution of a highly processive recombinant human dynein complex.* EMBO J, 2014. **33**(17): p. 1855-68.
23. Splinter, D., et al., *BICD2, dynactin, and LIS1 cooperate in regulating dynein recruitment to cellular structures.* Mol Biol Cell, 2012. **23**(21): p. 4226-41.

24. Kendrick, A.A., et al., *Hook3 is a scaffold for the opposite-polarity microtubule-based motors cytoplasmic dynein-1 and KIF1C.* J Cell Biol, 2019. **218**(9): p. 2982-3001.
25. Bullock, S.L., *Messengers, motors and mysteries: sorting of eukaryotic mRNAs by cytoskeletal transport.* Biochem Soc Trans, 2011. **39**(5): p. 1161-5.
26. McClintock, M.A., et al., *RNA-directed activation of cytoplasmic dynein-1 in reconstituted transport RNPs.* Elife, 2018. **7**.
27. Maldonado-Baez, L. and J.G. Donaldson, *Hook1, microtubules, and Rab22: mediators of selective sorting of clathrin-independent endocytic cargo proteins on endosomes.* Bioarchitecture, 2013. **3**(5): p. 141-6.
28. Luiro, K., et al., *Interconnections of CLN3, Hook1 and Rab proteins link Batten disease to defects in the endocytic pathway.* Hum Mol Genet, 2004. **13**(23): p. 3017-27.
29. Bielska, E., et al., *Hook is an adapter that coordinates kinesin-3 and dynein cargo attachment on early endosomes.* J Cell Biol, 2014. **204**(6): p. 989-1007.
30. Guo, X., et al., *Rab5 and its effector FHF contribute to neuronal polarity through dynein-dependent retrieval of somatodendritic proteins from the axon.* Proc Natl Acad Sci U S A, 2016. **113**(36): p. E5318-27.
31. Xu, L., et al., *An FTS/Hook/p107(FHIP) complex interacts with and promotes endosomal clustering by the homotypic vacuolar protein sorting complex.* Mol Biol Cell, 2008. **19**(12): p. 5059-71.
32. Lenz, J.H., et al., *A dynein loading zone for retrograde endosome motility at microtubule plus-ends.* EMBO J, 2006. **25**(11): p. 2275-86.
33. Abenza, J.F., et al., *Long-distance movement of Aspergillus nidulans early endosomes on microtubule tracks.* Traffic, 2009. **10**(1): p. 57-75.
34. Wedlich-Soldner, R., et al., *A balance of KIF1A-like kinesin and dynein organizes early endosomes in the fungus Ustilago maydis.* EMBO J, 2002. **21**(12): p. 2946-57.
35. Zekert, N. and R. Fischer, *The Aspergillus nidulans Kinesin-3 UncA Motor Moves Vesicles Along a Subpopulation of Microtubules.* Mol Biol Cell, 2008. **20**(2): p. 673-84.
36. Baumann, S., et al., *Endosomal transport of septin mRNA and protein indicates local translation on endosomes and is required for correct septin filamentation.* EMBO Rep, 2014. **15**(1): p. 94-102.
37. Baumann, S., et al., *Kinesin-3 and dynein mediate microtubule-dependent co-transport of mRNPs and endosomes.* J Cell Sci, 2012. **125**(Pt 11): p. 2740-52.
38. Higuchi, Y., et al., *Early endosome motility spatially organizes polysome distribution.* J Cell Biol, 2014. **204**(3): p. 343-57.
39. Salogiannis, J., M.J. Egan, and S.L. Reck-Peterson, *Peroxisomes move by hitchhiking on early endosomes using the novel linker protein PxdA.* J Cell Biol, 2016. **212**(3): p. 289-96.
40. Guimaraes, S.C., et al., *Peroxisomes, lipid droplets, and endoplasmic reticulum "hitchhike" on motile early endosomes.* J Cell Biol, 2015. **211**(5): 945-54.
41. Salogiannis, J. and S.L. Reck-Peterson, *Hitchhiking: A Non-Canonical Mode of Microtubule-Based Transport.* Trends Cell Biol, 2017. **27**(2): p. 141-150.
42. Mogre, S.S.C., J.R.; Niman, C.S.; Reck-Peterson, S.L.; and Koslover, E.K. , *Hitching a ride: mechanics of transport initiation through linker-mediated hitchhiking.* . Biophysical Journal, 2020: p. **in press**.
43. Lin, C., et al., *Active diffusion and microtubule-based transport oppose myosin forces to position organelles in cells.* Nat Commun, 2016. **7**: p. 11814.
44. Liao, Y.C., et al., *RNA Granules Hitchhike on Lysosomes for Long-Distance Transport, Using Annexin A11 as a Molecular Tether.* Cell, 2019. **179**(1): p. 147-164 e20.
45. Haag, C., B. Steuten, and M. Feldbrugge, *Membrane-Coupled mRNA Trafficking in Fungi.* Annu Rev Microbiol, 2015. **69**: p. 265-81.
46. Cioni, J.M., et al., *Late Endosomes Act as mRNA Translation Platforms and Sustain Mitochondria in Axons.* Cell, 2019. **176**(1-2): p. 56-72 e15.
47. Jansen, R.P., et al., *mRNA transport meets membrane traffic.* Trends Genet, 2014. **30**(9): p. 408-17.
48. Gohre, V., et al., *Microtubule-dependent membrane dynamics in Ustilago maydis: Trafficking and function of Rab5a-positive endosomes.* Commun Integr Biol, 2012. **5**(5): p. 485-90.
49. Pohlmann, T., et al., *A FYVE zinc finger domain protein specifically links mRNA transport to endosome trafficking.* Elife, 2015. **4**.
50. Steinberg, G., *The mechanism of peroxisome motility in filamentous fungi.* Fungal Genet Biol, 2016. **97**: p. 33-35.
51. Schinke, J., et al., *The DenA/DEN1 Interacting Phosphatase DipA Controls Septa Positioning and Phosphorylation-Dependent Stability of Cytoplasmatic DenA/DEN1 during Fungal Development.* PLoS Genet, 2016. **12**(3): p. e1005949.
52. Egan, M.J., K. Tan, and S.L. Reck-Peterson, *Lis1 is an initiation factor for dynein-driven organelle transport.* J Cell Biol, 2012. **197**(7): p. 971-82.
53. Christmann, M., et al., *Control of multicellular development by the physically interacting deneddylases DEN1/DenA and COP9 signalosome.* PLoS Genet, 2013. **9**(2): p. e1003275.
54. Meijer, W.H., et al., *Peroxisomes are required for efficient penicillin biosynthesis in Penicillium chrysogenum.* Appl Environ Microbiol, 2010. **76**(17): p. 5702-9.
55. Welte, M.A., *Expanding roles for lipid droplets.* Curr Biol, 2015. **25**(11): p. R470-81.
56. Szewczyk, E., et al., *Fusion PCR and gene targeting in Aspergillus nidulans.* Nat Protoc, 2006. **1**(6): p. 3111-20.
57. Nayak, T., et al., *A versatile and efficient gene-targeting system for Aspergillus nidulans.* Genetics, 2006. **172**(3): p. 1557-66.
58. Lee, S.B. and J.W. Taylor, *Isolation of DNA from fungal mycelia and single spores.*, in *PCR Protocols: A Guide to Methods and Applications* D.G. M. Innis, J. Sninsky and T. White , eds., Editor. 1990, Academic Press, Orlando, Florida. p. 282-287.
59. Gibson, D.G., et al., *Enzymatic assembly of DNA molecules up to several hundred kilobases.* Nat Methods, 2009. **6**(5): p. 343-5.
60. Straubinger, B., Straubinger, E., Wirsel, S., Turgeon, G., and Yoder, O.C. , *Versitile fungal transformation vectors carrying the selectable bar gene of Streptomyces hygroscopicus.* Fungal Genetics Newsletter, 1992. **39**: p. 82–83.
61. Todd, R.B., M.A. Davis, and M.J. Hynes, *Genetic manipulation of Aspergillus nidulans: meiotic progeny for genetic analysis and strain construction.* Nat Protoc, 2007. **2**(4): p. 811-21.
62. Subach, O.M., et al., *Conversion of red fluorescent protein into a bright blue probe.* Chem Biol, 2008. **15**(10): p. 1116-24.
63. Shcherbo, D., et al., *Far-red fluorescent tags for protein imaging in living tissues.* Biochem J, 2009. **418**(3): p. 567-74.
64. Suresh, S., et al., *Tools for retargeting proteins within Aspergillus nidulans.* PLoS One, 2017. **12**(12): p. e0189077.
65. Shevchenko, A., et al., *Mass spectrometric sequencing of proteins silver-stained polyacrylamide gels.* Anal Chem, 1996. **68**(5): p. 850-8.